# NEW TECHNIQUES FOR RESOLUTION ENHANCEMENT IN 3D X-RAY TOMOGRAPHIC IMAGING FROM INCOMPLETE DATA

V.Vengrinovich[1], S.Zolotarev[1], Y.Denkevich[1] and G.-R.Tillack[2]
[1]Institute of Applied Physics; Minsk; Belarus; [2]Federal Institute for Materials Research and Testing (BAM); Berlin; Germany

**Abstract:** Accurate evaluation of dimensions directly from tomographic images, restored from only few x-ray projections, made in a limited observation sector, is considered exploiting pipes wall thickness assessment like a typical example. Both experiments and simulations are used to extract main errors sources. It is taken from as known, that neglecting of the scattered radiation and beam hardening effects results in image blurring, strong artifacts and finally inaccurate sizing. The computerized technique is developed to simulate the contribution of scattered radiation and beam hardening for the purpose of their further extraction from projected data. After those accompanying effects extraction the iterative Bayesian techniques are applied to reconstruct images from the projections, using volumetric and/or shell representation of the objects like pipes. The achieved error of virtual pipe wall thickness assessment from 3D images can be as small as $300\mu k$ comparing to 1mm provided by modern techniques. Finally the conclusion was drawn that standard projection techniques using X- or Gamma rays in combination with X-ray film or imaging plates can be applied for the data acquisition to reconstruct finally wall thickness profiles in an in-field environment.

**Introduction**: An accurate assessment of the pipe wall thickness, decreased by metal loss due to corrosion, cavitation, erosion, etc., is an important task in various industrial sectors like chemical, petrochemical or power engineering to ensure the safe operation of the constructions and to prevent hazards or damages. Accordingly several non-destructive testing (NDT) techniques have been developed allowing wall thickness assessment and flaw detection over the years. The techniques that are in use for this purpose today, like eddy-current, magnetic, ultrasonic, and X-ray techniques, are summarized in Tab. 1.

All techniques reviewed in Tab. 1, except those based on radiography (8,9), apply sensors which either are inserted in the inspected pipe or require direct contact with inner or outer surface of the pipe (like 5 and 6).

Table 1: NDT techniques for wall thickness assessment and flaw detection.

| No | Technique | Testable Materials | Refer. | Detected Defects |
|----|-----------|--------------------|--------|--------------------|
| 1 | Conventional Eddy-Current | Conductor | [1,2] | Pits, cracks, wall loss |
| 2 | Rotating and Multi Coil Probes | Conductor | [2-4] | Cracks, surface breaking |
| 3 | Remote Field Eddy-Current Technique | Thick Ferromagnetica | [2,4-6] | Wall loss |
| 4 | Magnetic Flux Leakage | Thick Ferromagnetica | [2] | Pits and wall loss |
| 5 | Ultrasonic IRIS | No limitations | [2,4] | Large pits and wall loss |
| 6 | Ultrasonic Lamb Waves | No limitations | [2,4,7] | Large pits and wall loss |
| 7 | Laser Optics | No limitations | [4] | Inner diameter |

| | | | | discontinuity. |
|---|---|---|---|---|
| 8 | Digital Radiography | No limitations | [8] | Tangential wall loss estimate |
| 9 | Planar Tomography | No limitations | [9] | Pits, cracks |

X-ray tomographic imaging of both the outer and the inner pipe surface could yield a non-contact and non-invasive solution of the stated problem, but regular CT is not applicable due to the restricted access to the pipe. For radiographic techniques film and digital detectors like imaging plates or flat panel detectors are available for image recording as well as gamma sources like Ir-192, which are commonly in use for pipes exposure because of the limitations of X-ray energies and wall thickness range. The aim of this article is to discuss two new image reconstruction techniques, based on the principles of the multi-step tomography (MST) [10-12] given a limited number of projections and restricted access for observation for both 2D and 3D applications. The problem is aggravated by a strong beam hardening and scattering effects contribution to the to the projection image Other restrictions appear from economic demands like minimizing the number of X-ray exposures within a restricted observation angle, which is usually less then 90°. The objective of this paper is to demonstrate with the example of corroded pipes the capabilities of the new computer based techniques for the image reconstruction from incomplete and noisy data. Some examples made with real pipes illustrate the attempts to use absolute minimum of only two cone-beam projections to provide accurate image reconstruction.

**Results:** 1. Unconstrained 3D Image Reconstruction using a surface representation of the object.

Consider the nonlinear operator equation

$$A(R(M)) = F \qquad (1)$$

where $F$ is the set of measured data for all $N$ projections: $F = \{f_n^m\}; n = 1, \Lambda, N$ with the measured data $f_n^m(p)$ in projection $n$, $\{p_j^n : j = 1, \Lambda, J_n\}$ the pixel position in projection $n$, $J = \sum_n J_n$ the total number of pixels at all projections, $R(M)$ the radius vector of the current point of the inner surface, $M(x, y, z) : \{M_i : i = 1, \Lambda, I\}$ the location of inner surface grid knots. The operator $A$ describes the correlation between the inner surface $S$ and the optical density at the projection given by the attenuation law. The geometrical setup of the data acquisition system is shown in fig. 1.

Two hulls represent the reconstructed object: outer and inner. The outer hull is assumed to be a cylinder with known radius. The inner surface is considered as a set of elementary surface elements $S_u : u = 1, \Lambda, U, S = YS_u, S_{u_1} \text{ I } S_{u_2} = 0, u_1 \neq u_2$ given by triangle with vertexes defining the nodes of a discrete grid. Let assign the projection of the surface element $S_u$ in the $n$-th detector plane as $\sigma_u^n$. The partition of the surface is implemented such that the osculating sides of adjacent triangles and their common vertexes belong only to one of the vertexes.

The direct operator sequentially searches through all inner hull elements for:
 (a) determination of the projection of triangle $S_u$ on the current detector plane
 (b) definition of triangle boundaries
 (c) selection of all pixels $p_j^n : j = 1, \Lambda, J_n$ with the center located inside the triangle $\sigma_u^n$ or on its boundaries
 (d) search for the cross points of the rays, passing through the inner and boundary pixels of the triangle $\sigma_u^n$, with the inner and outer object surface.

The ray sums $f_n^c(p)$ for pixel $p_j^n : j = 1, \Lambda, J_n$, defining the corresponding ray, are calculated as the distances between corresponding pairs of points. Hence the ray sums can be determined after calculating the forward operator $A(\boldsymbol{R}(M))_n = f_n^c(p), n = 1, \Lambda, N$. The functional

$$\delta_n(\boldsymbol{R}(M)) = \sum_{p_1^n}^{p_{J_n}^n} |f_n^c(p) - f_n^m(p)| / \sum_{p_1^n}^{p_{J_n}^n} f_n^m(p) \qquad (2)$$

represents the difference between the current inner surface $S$, which is given by a set of discrete grid knots $M_i, i = 1, \Lambda, I$, and the inner surface, being the best fit to measured data.

The iteration procedure for reconstructing the inner surface is implemented continuously. The displacement takes place along the direction perpendicular to the line connecting the node $M_i$ with the coordinate axis. The specimen in the fig.1 represents a complex pipe structure built from two half-shells with 2 horizontal and 5 vertical holes, one circumferencial notch and four axial wires with diameters from 0.8 to 1.6 mm.
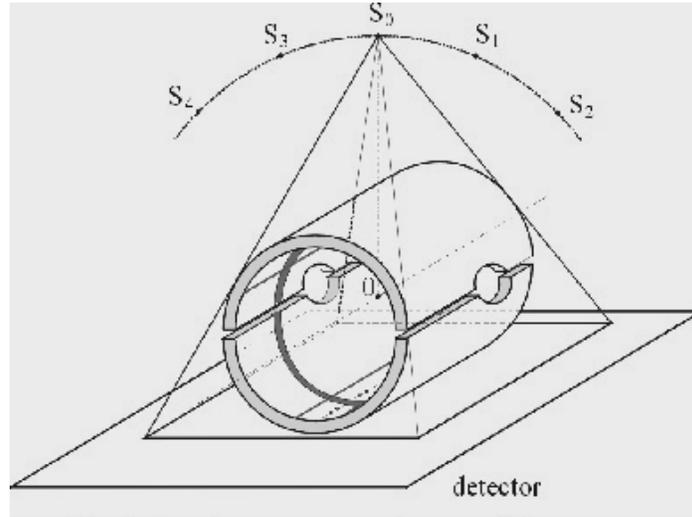


Fig.1. Cone-beam geometry data acquisition

For the exposure an Ir-192 source with a focus of 3 mm is used. A total of five projections are recorded from the five source positions shown in fig. 1, which are located within an angle of 90° choosing steps of 22.5°. Imaging plates are used for image recording with pixel size of 56 μm and a dynamic range of 12 bit. The complete 3-D image of the object is reconstructed on standard PC hardware. The result of reconstruction is shown in fig. 2 together with the profiles marked in the image.

2. Bayesian Pipe's Image Reconstruction considering scattering effect.

Consider a pipe under in service condition, i.e. the pipe is covered by insulation and filled with a work liquid. Supposing all absorbed radiation components are multiplicative for the filled and insulated pipe:

$$I_a = I_0 \exp\left[-\left(\mu_p l_p + \mu_i l_i + \mu_l l_l\right)\right], \qquad (3)$$

where $I_a$ is the primary intensity, $l_i(x)$ and $l_l(x)$ give the ray length in the insulation and liquid respectively.

Additionally it is assumed that the absorbed, scattered and background contributions are additive. Then the process of radiation propagation is described by

$$I(x) = I_0(x) \exp\left\{ -\sum_{i=0}^{3} \mu_i(l_i(x))l_i(x) \right\} + I_s(x) + I_b(x) \tag{3}$$

where $I(x)$ is the total intensity in the detector plane (normalized dose), i.e. the sum of primary, scattered, and background radiation.
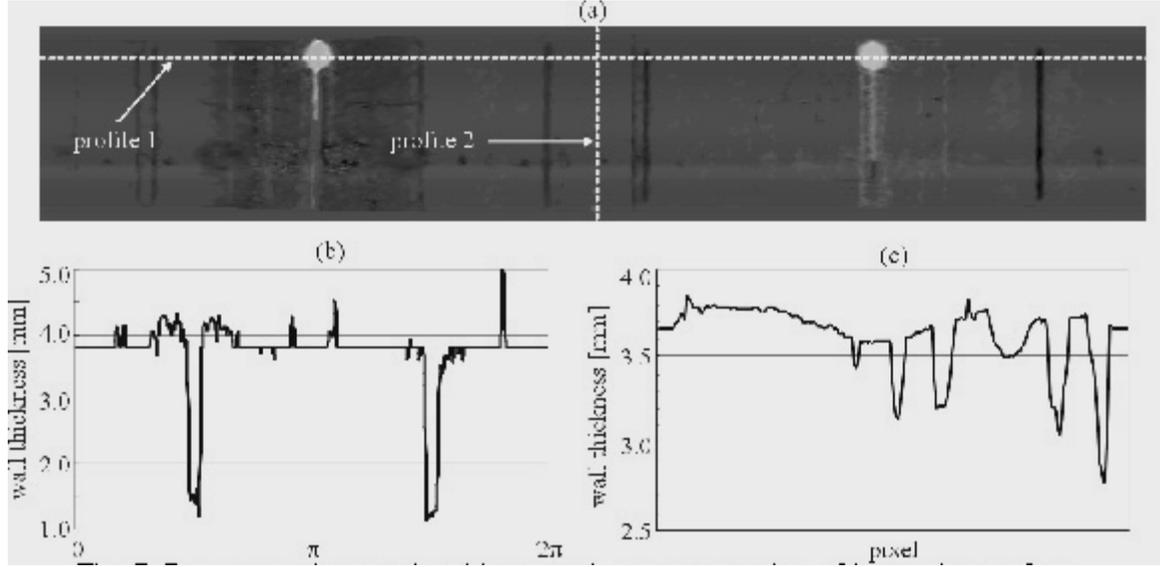


Fig.2. Reconstruction results: a) gray value representation of the inner pipe surface together with circumferential wall thickness profile 1 and profile 2 along pipe axis shown in b) and c) respectively.

3. Scattering effect and background:

The contribution of scattered radiation to the total radiation in the detector plane for the case, investigated here, has been estimated applying standard Monte Carlo packages for photon transport [13]. The idea, exploited in this elaboration in order to extract the scattered radiation from the total measured, assumes to approximate the profile of scattered radiation across the pipe axis by the Gaussian-type function. The parameters of the Gaussian distribution can be estimated from the measurements taken from a perfect pipe at the same experimental setup. The resulting profile signed as 4 in fig. 3 comes out after extraction of the simulated scattered profile 3, received after approximation of the scattered profile 5, from the total measured profile 1. The approximation is implemented using the following equation:

$$I_s = a \exp\left( \frac{x^2}{b} \right) \tag{4}$$

where $a$ and $b$ are the unknown constants calculated using data from the perfect pipe.

If a pipe with insulation and filling medium is assumed additional contributions to the scattered radiation have to be considered providing additive contributions from the three parts

$$I_s = I_{sp} + I_{si} + I_{sl} \tag{5}$$

where $I_{sp}$, $I_{si}$ and $I_{sl}$ give the scattered radiation from the pipe, the insulation, and the filling medium, respectively.

If flat panel detectors are used for image recording the contribution of the background can be calculated by extracting the "black" and "white" images from the raw data. But if using films or imaging plates the background is unknown. By analyzing multiple images of reference pipes the assumption of a linear approximation of the background radiation can be made. The two parameters of the linear function are taken from the profile under consideration by analytical continuation in the pipe projection area.

$$I_b = c(x+T) \; ; \; -T \le x \le T \tag{6}$$

where $c$ is a unknown constant calculated from the data of the current pipe, and $I_b$ gives the background intensity.

4. Determination of the parameter $I_0$ in equation (3).

To determine $I_0$ an appropriate signal transformation has to be implemented considering possible non-linearities of the detector and the beam hardening effects. The transfer function of the used fluorescence screen / film system is usually nonlinear but can be estimated experimentally. It can be represented as a plot of the optical density function versus the radiation dose (exposure time) for the corresponding screen/film system. A simple procedure is proposed to handle the non-linearity of this function meeting reasonable calculation simplicity. The $D(t)$-function in this application range is approximated by a linear function.

5. Extraction of the scattered radiation and background.

The extraction of the scattered radiation from the profile is provided by subtracting the calculated primary intensity $I_a(x)$ from the experimental profile $I(x)$. Finally the sum of two functions is evaluated:

$$I^{'}(x) = I_s + I_b = a\exp\left(-\frac{x^2}{b}\right) + c(x+T) \tag{7}$$

6. Calculation of the unknown coefficients a, b and c.

In the next step the extraction of the scattered radiation and background is possible applying eq. (3). This step is necessary in order to interpret the experimental data after this extraction in the form of linear attenuation model (3).

Based on previous reasoning the unknown coefficients $a$, $b$ and $c$ can be calculated. For this purpose the following optimization procedure is applied, making use of the real measurements taken from a perfect pipe with:

$$\{\widetilde{a},\widetilde{b},\widetilde{c}\} = \arg\min\left\{\sum_i \left[I_i^{'calc} - I_i^{'meas}\right]^2 : (a,b,c) \in R^n\right\} \tag{8}$$

where the superscripts at $I^{'}$ point on calculated intensities using eq. (7) and measured values, respectively. $R^n$ gives the admissible space for the unknown coefficients.

7. Image reconstruction and wall thickness measurements of a pipe.

To illustrate the proposed technique the results of real x-ray exposures of the perfect pipes with known geometry as well as dual projections data made with the pipe phantom with a given defect[1] are investigated.

Figs. 3a shows the x-ray profiles of 100x4,1 mm phantom pipe without insulation and filling. In all cases a Ir-192 gamma source and an RCF / FD8p screen/film system (AGFA) was used for exposures. Profile 1 gives the measured and digitized asymmetric profile after preprocessing. Taking two points of the profile as the reference points it is possible to approximate the background by linear interpolation with eq. (7) and to calculate the coefficients $c$ and $d$. The background profiles are shown by curves 2. By extracting the background profile from the measured data the corrected profile is received. This profile is symmetric with regard to the minimums, which approximately correspond to the tangential projection of the inner pipe wall (not shown).

In the next step the primary radiation profile 4 is simulated, which is a routine procedure if the dimensions of the pipe and the acquisition set up is known using eq. (3). Extracting the primary radiation profile from the corrected profile yields the scattered radiation profile. An example is shown by profile 5. The approximation of the scattering profile assumes a Gaussian-type function (4) with the coefficients *a* and *b* being calculated. The resulting simulated scattering profile is shown in figs. 3a, profile 3. This approximation of the scattering profile received from the phantom is used for the reconstruction of an unknown pipe images. The use of this profile gains advantages for the 2D and 3D image reconstruction compared to exploiting the preprocessed profiles of type 1 or after additional background correction (type 4), as known from experience. While investigating unknown pipes, the proposed procedure provides:

(i)     the measured profile after preprocessing (described in sections 3.2 and 3.3),

(ii)    the extraction of the background,

(iii)   the extraction of the scattered radiation, and

(iv)    the implementation of pipe image reconstruction according to the procedure described in sections 3.2 and 3.3. The entire procedure runs automatically.
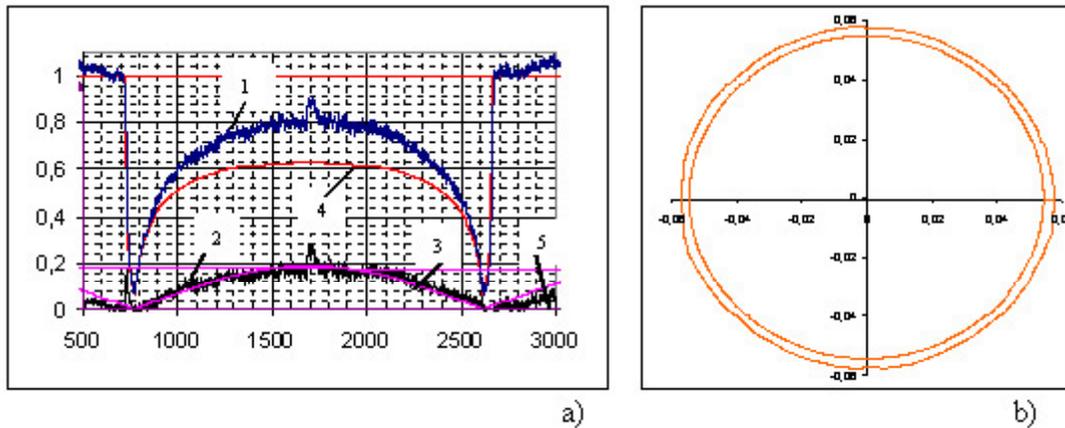


Fig.3. 100x4.1 pipe with the inner 6x3 notch in the down center pipe's part. a) X-ray radiation profile after pre processing: 1 – measured profile; 2 – simulated background radiation; 3 – simulated scatter radiation; 4 – simulated primary radiation; 5 – extracted scatter radiation. b) reconstructed pipe image from extracted primary radiation data taken from two orthogonal projections.

**Discussion:** Investigating the results shown in fig.2 it follows that the average pipe wall thickness is restored with high accuracy. The estimated error of restoration does not exceed 200 μm. This value holds for smooth wall thickness variations as known from corrosion and erosion. The accuracy of the reconstruction of the notches is smaller. The error is estimated at the level of about 500 μm. It is understandable that the proposed algorithm can not restore through-wall holes due to the applied surface representation in the reconstruction algorithm. But this was not the focus task of the investigation.

In Fig. 3b the results of the reconstruction of the pipe's inner cross section using the original primary radiation profiles of type 4 is shown. Fig. 3 presents the 2D tomographic reconstruction result of the pipe image from two orthogonal projections, using the corrected profile, improved by extracting the scattered radiation. The error of reconstruction did not exceed the following values: averaged 0.29 mm ; maximum 0.36 mm, and minimum 0.13 mm, what is comparable to regular CT with 720 projections.

The series of experiments and the results of the tomographic pipe image reconstruction, presented above, demonstrate the capability of the proposed techniques to provide accurate wall thickness measurements having only two projections available.

**Conclusions:** Finally it turns out that the discussed reconstruction algorithm is capable to monitor wall thickness variations in pipes with accuracy sufficient to meet practical requirements. This technique overcomes the major restrictions of other radiographic methods, which usually allow only measurements at specific positions but do not access the minimal wall thickness on the circumference of the pipe.

References:

1. ASME, "Eddy Current Examination of Tubular Products", *ASME Boiler and Pressure Vessel Code,* Vol.V: *Nondestructive Examination,* New York, American Society of Mechanical Engineers, 1992.
2. Mark,J.T. and D.Anges, "Steam Generator Inspections with the CECCO Probe", EPRI Steam Generator NDE Workshop, Palm Beach, FL, 1997.
3. Anmol S. Birring, "Selection of NDT Techniques for Heat Exchanger Tubing", *Materials Evaluation*, V.59, No.3, 2001, pp.382-391.
4. Fisher,J.L., "Remote Field Eddy-Current Inspection", *ASM Handbook*, Vol.17, 1992, pp.195-201.
5. Alleyne, D. and P. Cawley, "The Long Range Detection of Corrosion in Pipes Using Lamb Waves," *Review of Progress in QNDE,* Vol.14B, Ed., D.O.Thompson and D.E.Chimenti, New York, NY, Plenum Press, 1995, pp.2073-2080.
6. Krzywosz,K., "Flaw Detection and Characterization in Heat Exchanger Tubing", EPRI report No. GC 111672, December 1998.
7. Gupta, Nand K., B.G.Isaacskn, „Near Real Time Inservice Testing of Pipeline Components",*Materials Evaluation*, V.59, No.1, 2001, pp.55-58.
8. Lunin, V., Podobedov, D., Ewert, U., Redmer, B., "Numerical Evaluation of Welded Tube Wall Profiles From Scanned X-Ray Line Source Data", *Review of Progress in QNDE,* Vol.20, Ed., D.O.Thompson and D.E.Chimenti, New York, NY, AIP, 2001, pp.537-544.
9. Schmidt, T.R., „History of the Remote Field Eddy-Current Inspection Technique", *Materials Evaluation*, V.47, No.1, 1989, pp.14-22.
10. Zscherpel, U., Ewert, U., Onel, Y., "New Concepts for Corrosion Inspection of Pipelines by Digital Industrial Radiology (DIR)", Proceedings of the 15th World Conference on NDT, on CD, paper idn. 325
11. V. Vengrinovich, Yu. Denkevich and G.-R. Tillack. Reconstruction of Three-Dimensional Binary Structures from an Extremely Limited Number of Cone-Beam x-ray Projections. Choise of Prior. *Journal of Phys., D: Applied Physics.* V.32 pp. 2505-2514, 1999
12. V. Vengrinovich, Yu. Denkevich, and G.-R. Tillack. Bayesian 3D x-ray reconstruction from incomplete noisy data. In book: Maximum Entropy and Bayesian Methods, ed. by W.von der Linden et. al., Kluwer Academic Publishers, pp. 73-83,1999.
13. Briesmeister, J. F. (ed.), *MCNP–A General Monte Carlo N–Particle Transport Code*, LANL Report LA–13709–M, Los Alamos, 2000